

Electronic Supplementary Information

Sulfur vacancy-induced reversible doping of transition metal disulfides via hydrazine treatment

Sang-Soo Chee,^a Chohee Oh,^a Myungwoo Son,^a Gi-Cheol Son,^a Hanbyeol Jang,^a Tae Jin Yoo,^a Seungmin Lee,^b Wonki Lee,^c Jun Yeon Hwang,^c Hyunyong Choi,^b Byoung Hun Lee^a and Moon-Ho Ham^{*a}

^aSchool of Materials Science and Engineering, Gwangju Institute of Science & Technology (GIST), 123 Cheomdangwagi-ro, Buk-gu, Gwangju 61005, Republic of Korea

^bSchool of Electrical and Electronic Engineering, Yonsei University, 50 Yonsei-ro, Seodaemun-gu, Seoul 03722, Republic of Korea

^cInstitute of Advanced Composites Materials, Korea Institute of Science and Technology (KIST), 92 Chudong-ro, Eunha-ri, Bondong-eup, Wanju-gun, Jeollabuk-do 55324, Republic of Korea

E-mail: mhham@gist.ac.kr

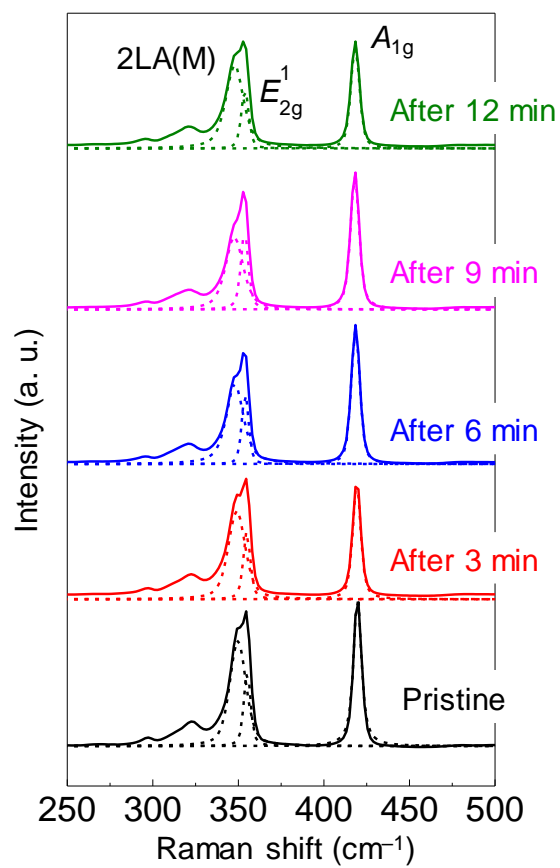


Figure S1. Raman spectra of WS₂ devices treated with hydrazine for different amounts of time.

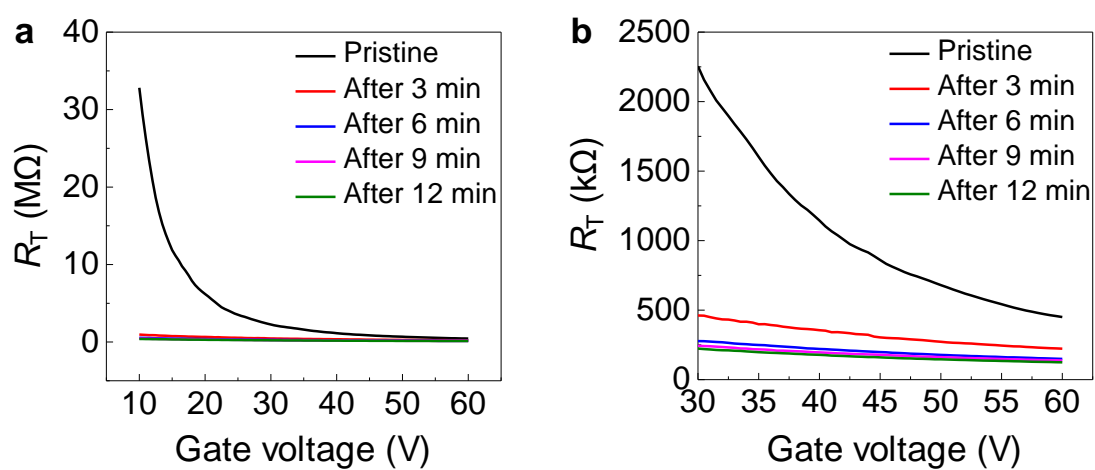


Figure S2. Total resistance (R_T) of WS₂ FETs. (a) R_T - V_G curves of WS₂ FETs treated with hydrazine for various amounts of time, obtained from I_{DS} - V_G curves in Fig. 2a. (b) Enlarged plots of the R_T - V_G curves in Fig. S2a.

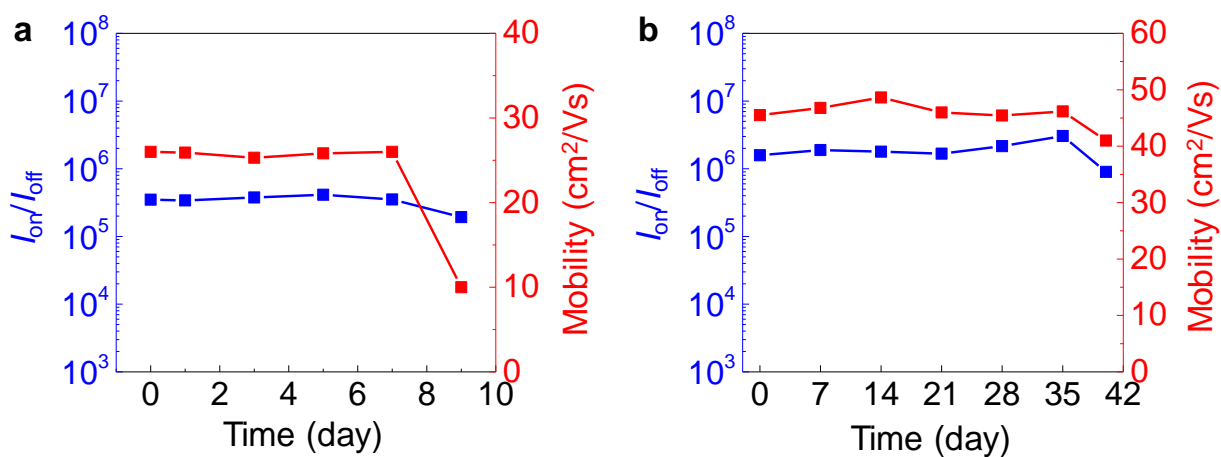


Figure S3. Doping stability of a hydrazine-doped WS₂ FET (a) without and (b) with a PMMA layer in ambient air. The on/off current ratio and field-effect mobility of the hydrazine-doped WS₂ FET covered with the PMMA layer remain almost unchanged in ambient air after even a month, demonstrating good air stability.

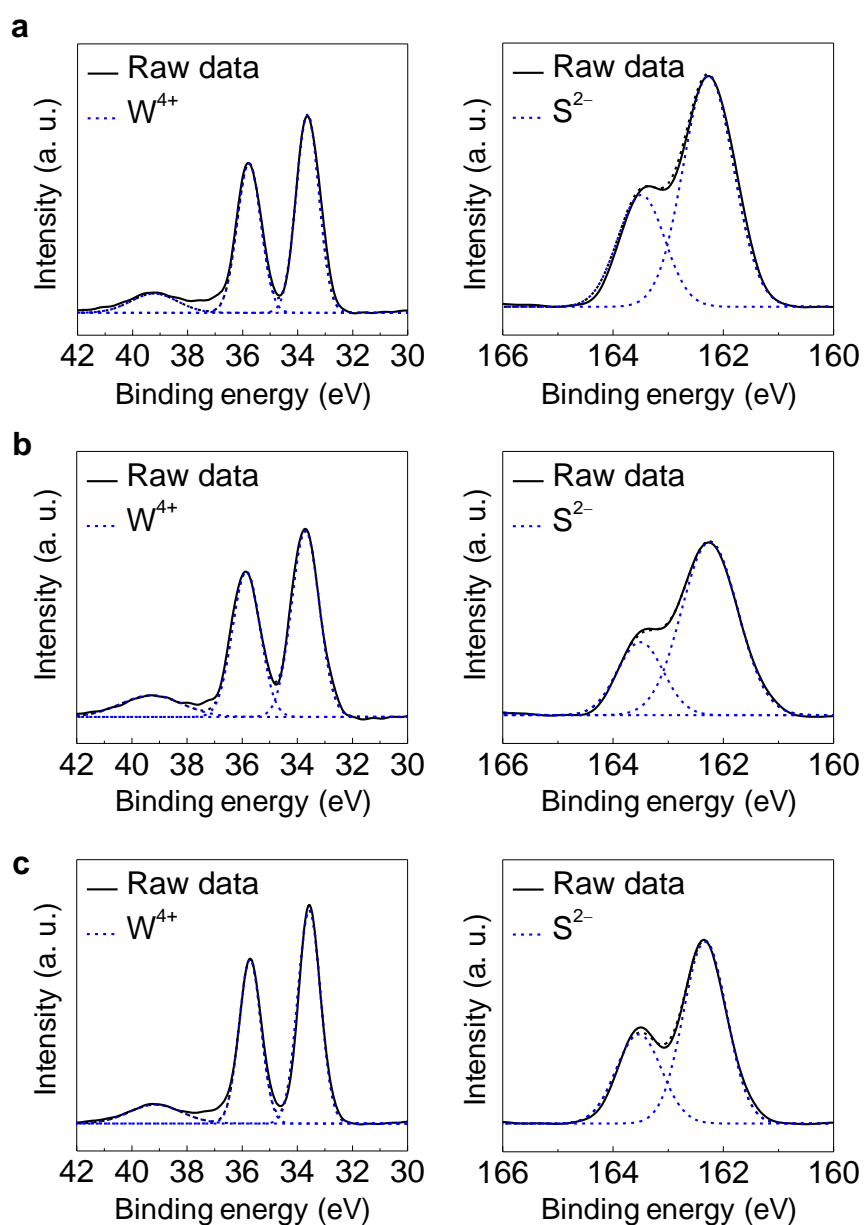


Figure S4. XPS spectra of W 4f and S 2p for (a) pristine, (b) hydrazine-doped, and (c) sulfur-annealed WS₂ flakes. Fitted curves of W 4f and S 2p spectra are represented as W⁴⁺ and S²⁻, respectively. Their S/W atomic ratios are estimated to be 1.90, 1.82, and 1.90 for pristine, hydrazine-doped, and sulfur-annealed samples, respectively.

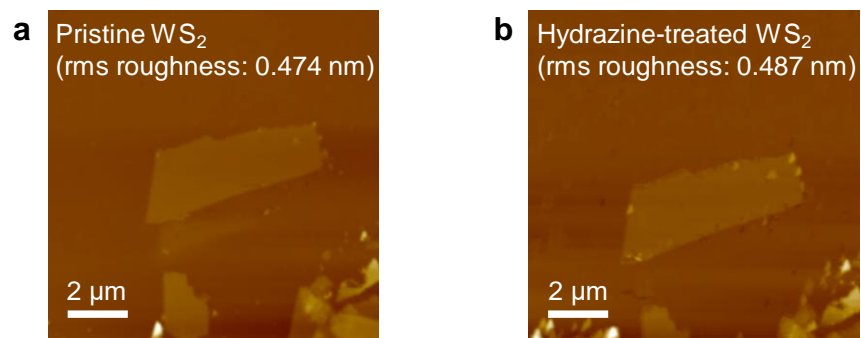


Figure S5. AFM images of WS₂ flakes (a) before and (b) after hydrazine treatment.

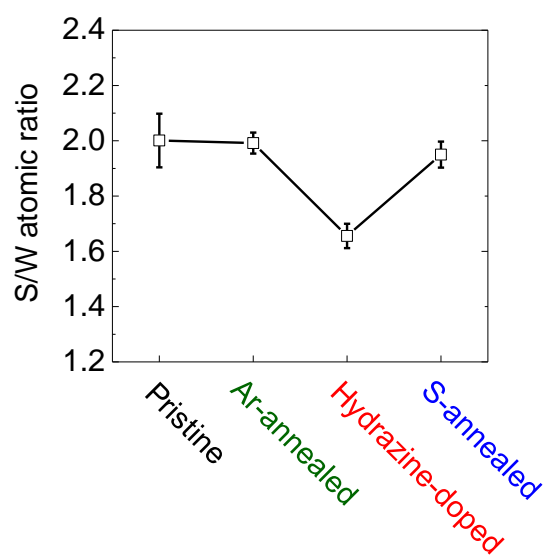


Figure S6. S/W atomic ratios for pristine, argon-annealed, hydrazine-doped, and sulfur-annealed WS₂ flakes, taken by EDX measurements.

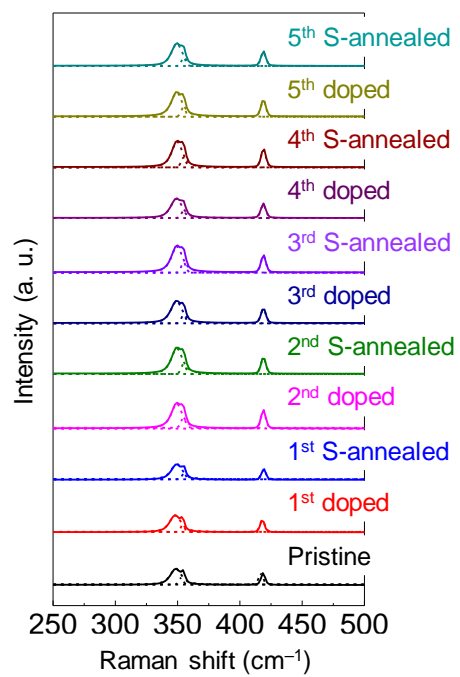


Figure S7. Raman spectra of a WS₂ flake upon five consecutive doping cycles, showing doping reversibility.

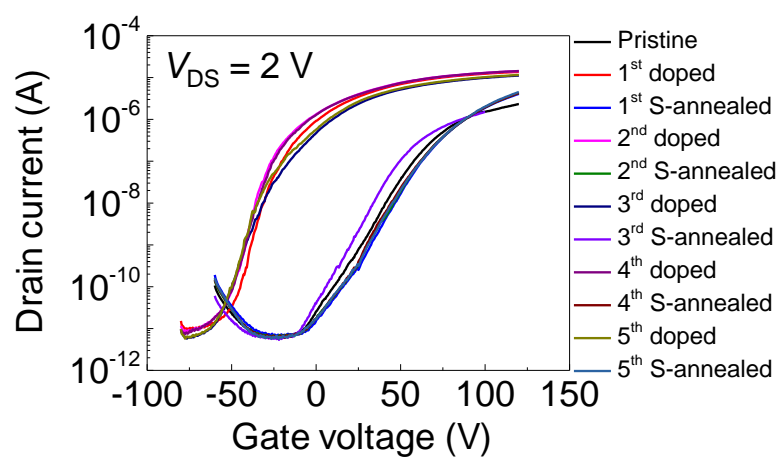


Figure S8. Transfer characteristics of a WS₂ FET upon five consecutive doping cycles, showing doping reversibility.

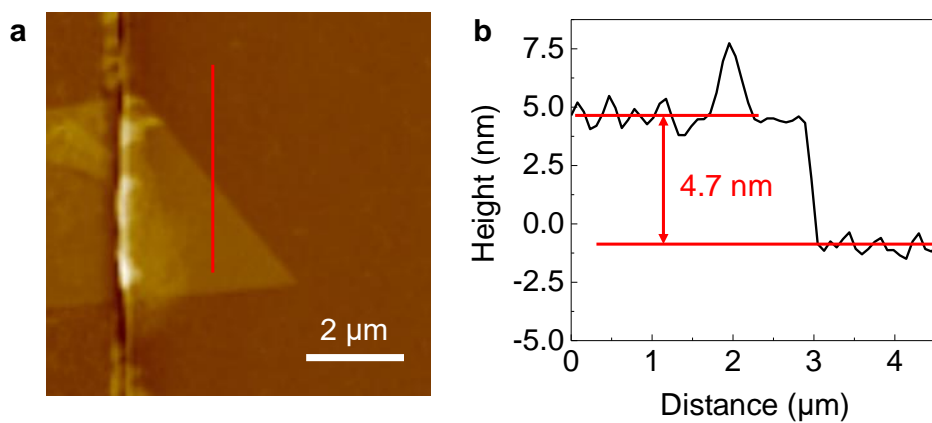


Figure S9. (a) AFM image and (b) thickness profile of a pristine MoS₂ FET.

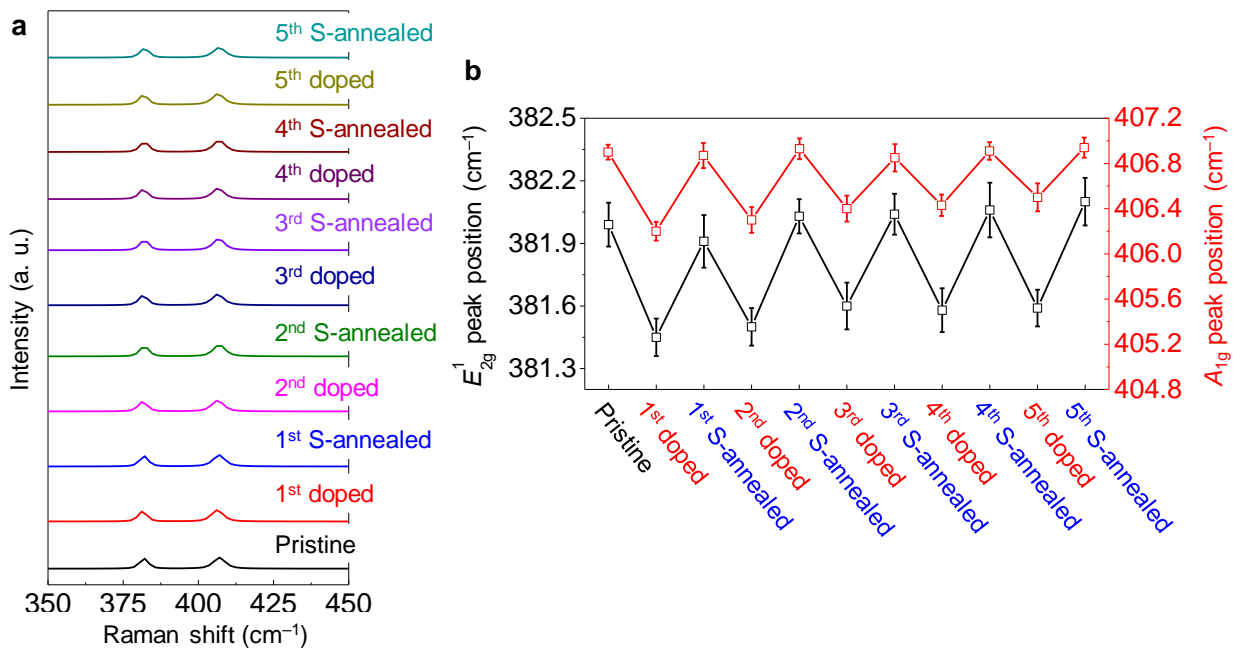


Figure S10. Raman spectra showing doping reversibility of MoS₂. (a) Raman spectra of a MoS₂ flake upon five consecutive doping cycles, and (b) variations in the E_{2g}^1 and A_{1g} peaks.

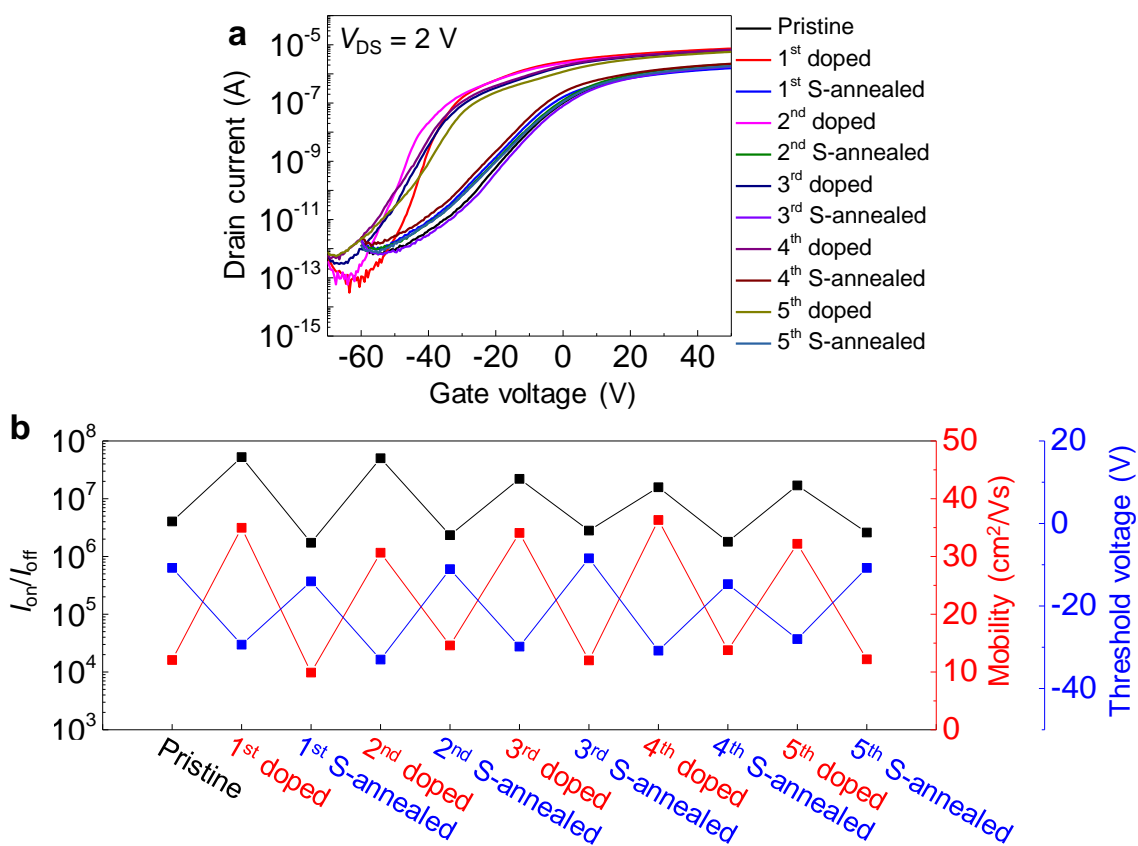


Figure S11. (a) Transfer characteristics and (b) variations in electrical properties including the on/off current ratio, field-effect mobility, and threshold voltage of a MoS₂ FET upon five consecutive doping cycles, showing doping reversibility.

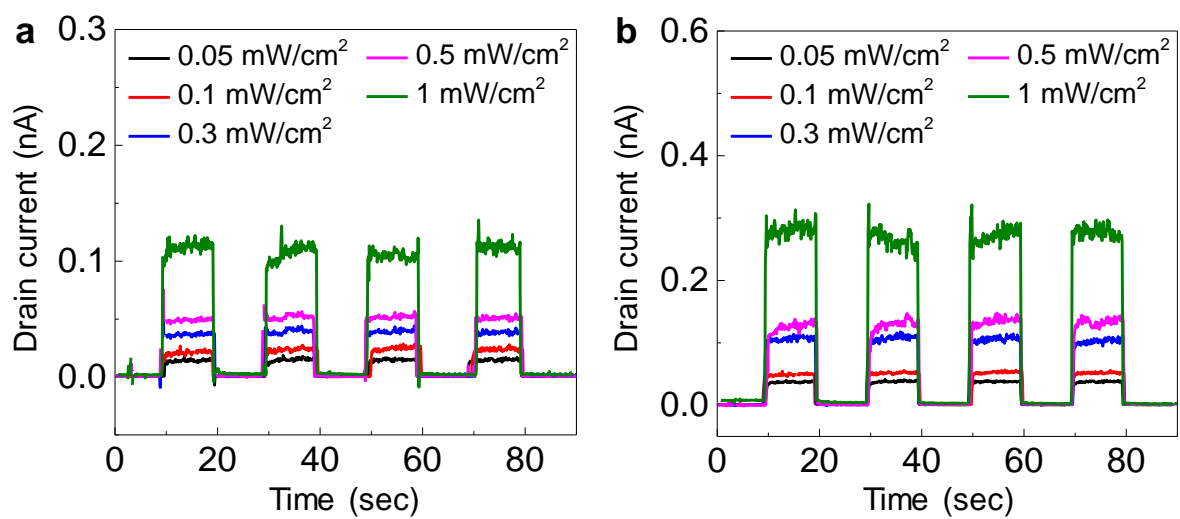


Figure S12. Time-dependent photoresponse characteristics of pristine WS₂ devices under irradiation with visible light of various power densities at 625 nm, measured at (a) $V_{DS} = 1$ V and (b) 2 V.

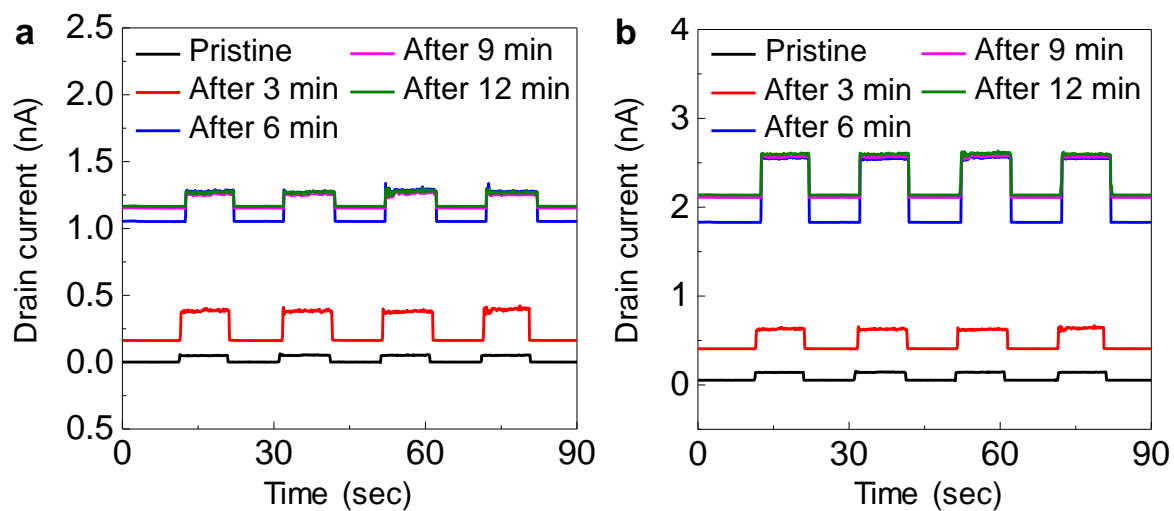


Figure S13. Time-dependent photoresponse characteristics of WS₂ devices treated with hydrazine molecules for different amounts of time, measured under irradiation with visible light at 625 nm and 1 mW cm⁻², and at (a) $V_{DS} = 1$ V and (b) 2 V.